Smooth Muscle Cell-Mimetic CO-Regulated Ion Nanochannels

Yanglei Xu, Xin Sui, Jiaqiao Jiang, Jin Zhai, and Longcheng Gao**

CO is traditionally regarded as a highly toxic gas, but it is also firmly regarded as an important gaseous messenger and physiological signaling molecule in the neuronal activities,[1] such as odor response adaptation, learning and memory, etc. In several tissues, endogenous CO is produced by enzymatic heme metabolism. It can bind directly to metal-containing proteins to interfere with intracellular signaling pathways and regulate different ion flux in channels.[2] For example, CO induces smooth muscle vasodilation by activating Ca^{2+}-activated K^+ channels. Heme acts as the inhibitor by binding to the amino acid sequence conserved in the channels. CO binds to heme with higher affinity. As CO is endogenously generated, CO binds dominantly to the heme, altering the interaction between heme and the amino acid in the channel (**Figure 1**a).[3] In this way, the inhibitory effect of the heme is removed by CO. The exposed acid groups in the channel facilitate the ions transport, leading to the increase of transient current, membrane hyperpolarization, and ultimately vasodilation.[4] The biological effect of CO relies on the interaction between CO and heme proteins.[5] Many diseases, including neurodegenerations,[6] inflammation,[7] have been linked to the CO function abnormality.

Inspired by the CO activated biological effect in smooth muscle cells, for the first of time, we apply the cellular principles into the construction of an artificial CO regulated ion nanochannel. The key factor is to establish a dynamic coordination system, where CO could tune the surface charge by altering the interaction between ferroporphyrin and carboxyl acid in the channels. Polyethylene terephthalate (PET) membrane is used to make conical asymmetric nanochannels for the ions transport. The nanochannels surface contains carboxyl groups and are intrinsically negative. They have the ability of transporting positive ions like K^+, Ca^{2+}. Ferroporphyrin is grafted onto the inner surface. Due to the coordination between ferroporphyrin and carboxyl acid, the ions transporting activity is inhibited by ferroporphyrin groups, similar with that in the cells. CO is used to release the carboxyl acid due to the higher affinity with ferroporphyrin. Therefore, the ions transporting ability is waken up. Herein, we demonstrate an artificial CO-gating system, which is exactly the same as that of the CO-regulated ion channel in nature. Meanwhile, because of the synergism between the conical asymmetric shape and the negatively charged surface of the inner nanochannels, the system emerges ion rectification, with the characteristics of the diodes. The nanofluidic diodes are regulated by CO.[8] Now the nanofluidic diodes have attracted wide interests in the fields such as biosensing,[9] proton pump,[10] and energy conversion system.[11]

The CO-gated nanodevices were produced on PET membranes. The interior surface of the nanochannels was modified with ferroporphyrin by one step coupling reaction between amino ferroporphyrin and carboxyl acid. The modification of ferroporphyrin was verified by X-ray photoelectron spectroscopy. Prior to modification, only C1s and O1s signal are detected. After modification, the appearance of N1s, Fe2p signals on PET surface, originating from ferroporphyrin, confirms the successful attachment of ferroporphyrin (see Figures S2–S4, Supporting Information).

The successful modification is also detected by the current–voltage (*I–V*) measurements. The corresponding *I–V* curves response for each steps of modification progress was examined by ion current at 0.1 mol L^{-1} of KCl solution. Before modification, the passing ions prefer to transport from tip to base because the sign of surface charge is negative, which could be attributed to the deprotonation of the carboxyl groups. Meanwhile, the system's ion current increases due to the lower resistance under the negative bias. The *I–V* curves show ion current rectification (**Figure 2**). The ion current rectification ratio is calculated by the absolute values of ion currents at a given voltage 2 V versus −2 V. The ion current rectification ratio calculated is ≈3.0, as the ion current is ≈−99.6 nA at −2 V and ≈32.9 nA at 2 V. With the ferroporphyrin immobilized on the nanochannels, the ion current decreased markedly. Moreover, the absolute values of ion currents at the voltages 2 and −2 V are close. The ion rectification disappears. The dramatical transition is attributed to the surface charge vanishment. After the ferroporphyrin modification, excess carboxyl acid groups remain due to the incomplete reaction. The carboxyl acid coordinates to the ferroporphyrin,[12] resulting in a close-to-neutral surface. The nanochannels varied from cation-selective to nonselective, the ion rectification vanishes, showing linear ion current behavior. The nanochannels turn to be a closed state.

The presence of ferroporphyrin on the nanochannels surface disables the ion transportation by associating the residual carboxyl acid groups. The bonding strength is not so high. The weak coordination is replaced by CO to form more stable complex, when CO is introduced.[13] **Figure 3**a shows the *I–V* curves of nanochannels after CO bubbling. A diode-like curve can be

Dr. Y. L. Xu, Dr. X. Sui, Dr. J. Q. Jiang,
Prof. J. Zhai, Prof. L. C. Gao
Key Laboratory of Bio-Inspired Smart Interfacial Science and Technology of Ministry of Education
Beijing Key Laboratory of Bio-Inspired Energy Materials and Devices
School of Chemistry and Environment
Beihang University
Beijing 100191, P. R. China
E-mail: zhaijin@buaa.edu.cn; lcgao@buaa.edu.cn

DOI: 10.1002/adma.201603478

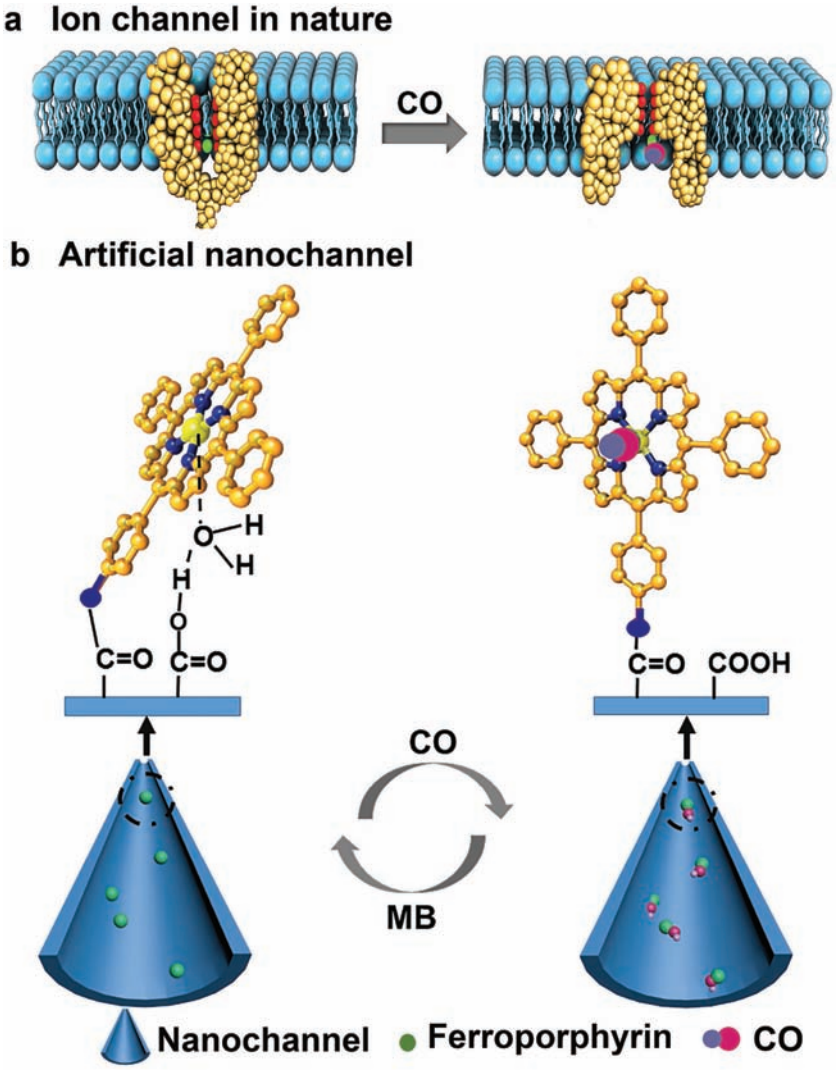

Figure 1. a) The scheme of the CO regulation ions transportation across cell membranes. CO induced cellular signaling leads to "ON-OFF" switch. b) Flow chart for CO activated nanochannel. CO binds to ferroporphyrin to release carboxyl acid on the nanochannel surface, leading to "ON" state. In turn, methylene blue (MB) removes CO from the ferroporphyrin–CO complex. The carboxyl acid attracts ferroporphyrin and the surface becomes neutral, resulting in the "OFF" state.

seen, which is similar with the *I–V* curve of unmodified one. After bubbling CO to the ferroporphyrin modified nanochannels, the ion current increases from –12.9 to ≈–57.8 nA at –2 V. The ion current rectification ratio reaches to 10.3 (Figure 3c); because CO interferes in the complex of ferroporphyrin and carboxyl groups, resulting in exposure of carboxyl acid groups on the surface. As results, the neutral surface turns to be negative (Figure S5, Supporting Information). The ion transporting ability is recovered. Just like the ion channels in cells, the ion nanochannels are opened by CO. If the nanochannels are not modified with ferroporphyrin, the *I–V* curves in the absence and presence of CO are more or less similar (Figure 3b). There are no significant ion current and ion current rectification changes. Because the surface charges density of the unmodified nanochannels cannot be changed by CO.

Here, the ferroporphyrin modified nanochannels demonstrate two dramatically different states of ON and OFF switched by CO. The gating ratio of CO sensing system after modification is much larger than that of nanochannels before modification, which testified that the ion gating was controlled by the binding reaction of CO and ferroporphyrin. The current ratio was 4.0, calculated by the ionic currents measured in the presence of CO versus the absence of CO at –2 V (Figure 3d). It was higher than 0.98 measured and calculated in nanochannels without ferroporphyrin modification. Thus, the biomimetic smart nanosystem exhibits excellent CO recognition capability reflected by both extremely high ion rectification ratio and ion gating ratio. The ferroporphyrin-modified nanochannels show high selectivity toward CO. The other gases, such as CO_2, N_2, do not exhibit the properties in Figures S6 and S7 (Supporting Information). The CO-recovering rate of the artificial ion nanochannels from the blockage state is fast. Within 15 s, the blocked nanochannels can be opened by CO.

The ion transport properties of the CO sensing system have also been examined by current measurements at different concentrations of KCl, NaCl, and $CaCl_2$, and all of them exhibit ion current rectification phenomenon. The ion current increases with the increase of concentration. All the *I–V* curves at different concentrations are shown in Figures S8–S12 and Table S1 (Supporting Information). The ion current at KCl solutions is found to be higher in comparison of $CaCl_2$ and NaCl solutions.

The CO responsive properties of the ferroporphyrin modified nanochannels are reversible, which is demonstrated by the addition and removal of CO.[14] **Figure 4**a shows the *I–V* curves of the ferroporphyrin modified nanochannels after bubbling CO and adding methylene blue (MB). After bubbling CO, the nanosystem changes from an OFF state to an ON state. When MB is added into the system, the *I–V* curve exhibits linear characteristics, and returns to the OFF state. MB has been known as an antidote to CO poisoning.[15] MB releases CO from the complex of ferroporphyrin–CO. Again, the released ferroporphyrin groups bind carboxyl acid groups, leading the surface of the nanochannels to be neutral. Thus, the ion nanochannels are blocked. Figure 4b shows ON/OFF switch upon alternating introduction of CO and MB, which reflects the reversibility and repeatability of the system.

It is worth to note that the chemical modification of nanochannels with ferroporphyrin is essential. In principle, the unmodified nanochannels can be blocked by ferroporphyrin with physical adsorption instead of chemical modification. We introduced ferroporphyrin without amino

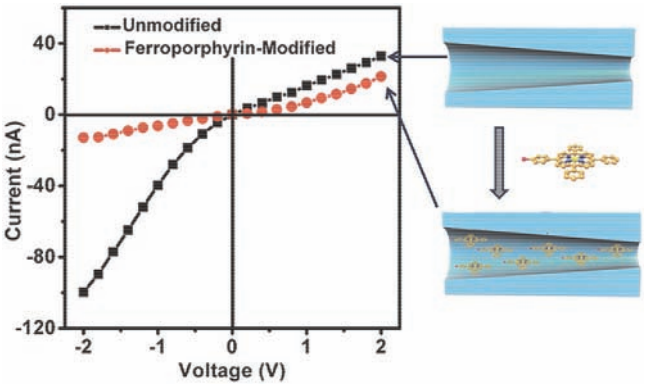

Figure 2. The *I–V* curves of the nanochannels before (square) and after (circle) ferroporphyrin modification (0.1 mol L^{-1} of KCl solution). The original nanochannels surface is negatively charged, exhibiting ion current rectification property. After ferroporphyrin modification, the surface gets neutralized and the ion current rectification vanishes.

junction group into the nanochannels surface by coordination between ferroporphyrin and carboxyl groups. The *I–V* curve shows linear characteristics (Figure S13, Supporting Information). However, CO recovers the ion current rectification behaviors irreversibly. After adding MB, the *I–V* curve does not change any more. That is because the ferroporphyrin is removed permanently from the surface by bubbling CO.

CO acts as the trigger for the opening of the ferroporphyrin modified nanochannels. After inducing CO, the nanochannels show the cation selectivity, which prefer the transportation of cations and inhibit the transportation of anions. Considering the synergistic effect of the asymmetric geometric structure and the surface charge, the nanochannels exhibit diode-like current. We simulate the nonlinear ion current behaviors by solving the Poisson and Nernst–Planck (PNP) equations.[16] The mechanism can be further theoretically supported by PNP equation and based on the fixed charge of the nanochannels, corresponding to the surface charge change before and after ventilating with CO to nanosystem.

PNP equation together with the steady state continuity equation[17]

$$J_i = -D_i\left(\nabla C_i + Z_i C_i \nabla\varphi\right) + C_i V_{\text{eof}},\ i = +, - \tag{1}$$

$$\nabla J_i = 0,\ i = +, - \tag{2}$$

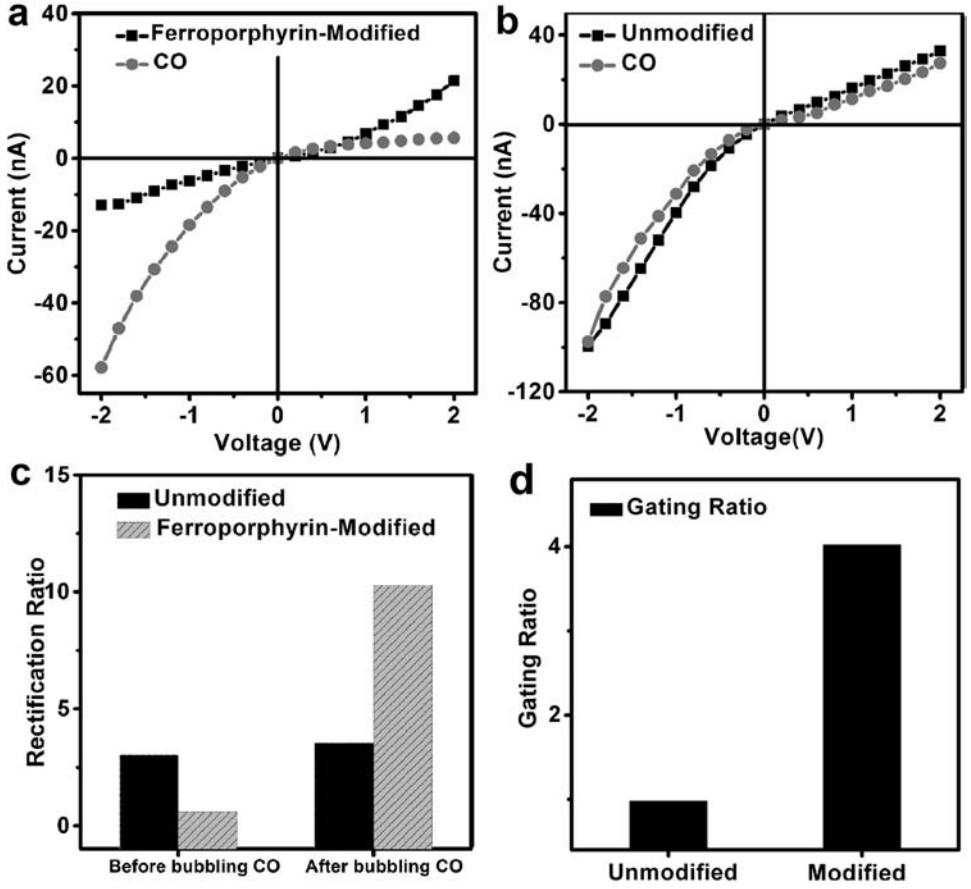

Figure 3. The current–voltage (*I–V*) curves of nanochannels a) with and b) without ferroporphyrin modification as a function of CO (0.1 mol L^{-1} of KCl solution). c) The ion rectification ratios and d) gating ratios show that the ferroporphyrin-modified nanochannels are opened by CO.

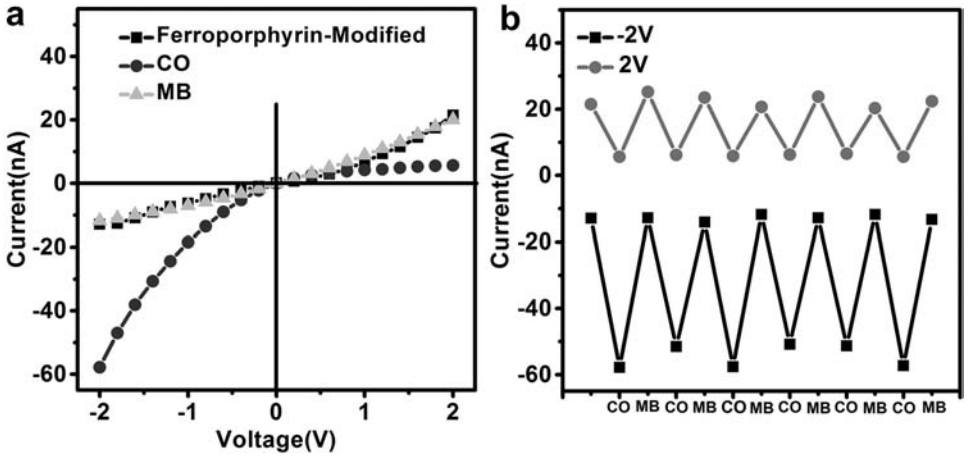

Figure 4. a) The contrast of *I–V* curves of ferroporphyrin-modified nanochannels at the original condition, after bubbling CO and adding MB, showing a reversible switchable multiple nanosystem. b) Reversible functionalized nanochannels exhibit ion current with bubbling CO and adding MB to solution for binding of ferroporphyrin at 2 and −2 V.

$$\nabla^2\varphi = \frac{F^2}{\varepsilon RT}(C_- - C_+) \tag{3}$$

Where *i* indicates anions or cations in this system (*i*+ stands for cations and *i*− stands for anions). J_i, C_i, φ, F, D_i, Z_i, V_{eof}, ε are the flux of ions, anion/cation concentration, electric potential, the Faraday constant, a diffusion coefficient, the charge number of anions/cations, electroosmotic velocity, and dielectric constant.

The ion current rectification model of this conical nanochannel built in the software COMSOL Multiphysics,[18] which applies the model of transport of diluted species and electrostatics. To build a simplified model, the 2D signal conical symmetry nanochannel model was stimulated. The below are the boundary conditions in this model; the model is along the center axis of nanochannel; the electrolyte solution concentration is $c_L = c_R = 0.1$ mol L^{-1} in this work; the thickness of membrane is 2.3 μm; the diffusion coefficients of anion and cation are set as 1.93×10^{-5} and 2.03×10^{-5} cm^2 s^{-1}.

Figure 5a presents the simulated *I–V* curves. Obviously, the system shows the ion rectification when the CO is applied. The surface density is defined as -1×10^{-4} C m^{-2}. After adding MB, the surface charge is reduced to minimum. The ion rectification vanishes, which obeys the Ohm law. Figure 5b shows the electric potential distribution in the nanochannel at −2 and 2 V before and after bubbling with CO, respectively. Before bubbling CO, the electric potential distribution is uniform. After bubbling CO, the electric potential distribution is nonuniform due to the asymmetric feature of the nanochannels. At −2 V, cations move to the base direction and anions move to the tip direction. The ion conductance and the ion current increase. At 2 V, the ion conductance and ion current decrease, because cations move to the tip direction. Therefore, the ion current is asymmetric, the system shows ion current rectification in accordance with our experimental data.

Figure 5c,d illustrates the cations concentration distributions in the nanochannel along the 2D axis under the negative bias at −2 V and the positive bias at 2 V. They show the cations concentration distributions at the surface density -1×10^{-4} C m^{-2} is larger than ones at the surface density at −2 and 2 V. When ventilating with CO, the existence of the surface negative charge on the channel walls results in the increase of the passing ionic concentrations in the channel along the pore central axis. The cations are attracted and anions are repelled due to the electrostatic potential. The synergistic effect of asymmetric channel and the negative surface charge of nanochannel wall induce accumulation of cations near the tip. Thus, the cation concentrations at −2 V is smaller than ones at +2 V. The simulation fulfills the CO-regulated ion current rectification properties in the nanochannels.

In conclusion, we report a CO gate-keeping capability of ion nanochannels system, which is consistent with the CO direct stimulatory effect in biological system. CO has been used as the trigger for controlling the ON and OFF states of the nanochannels. Furthermore, the CO gating system exhibits characters of reversibility and fast response rate. The PNP theoretical simulations agree with the CO-regulated ion transporting properties. These results help us understand the synergistic effect of the gaseous messengers in the ion channels of the living organisms, and also provide promising applications in the smart nanodevices, such as CO sensors.

Experimental Section

Nanochannels Fabrication: PET (thickness: 23 μm) was irradiated with an Au ion beam to form multiple cylindrical pores (5×10^8 cm^{-2} track density). Then, ion track etching technique was used to obtain conical nanochannels.[19] First, the membranes were irradiated under UV light (365 nm) for 2 h from both sides. Then, at 40 °C, the etching (NaOH, 9 mol L^{-1}) and the stopping solution (1 mol L^{-1} KCl and 1 mol L^{-1} HCOOH) were added in two different sides of the reaction cell for ≈50 min (Figure S14, Supporting Information). The etching process was monitored by the voltage (1 V). Pt electrode was applied to the etching process. The ion current was observed. When the transmembrane ionic current increased sharply, the nanochannels opened and presented the conical. The big size pores (base, ≈350 nm) of the nanochannels were observed by scanning electron microscopy (Figure S1, Supporting

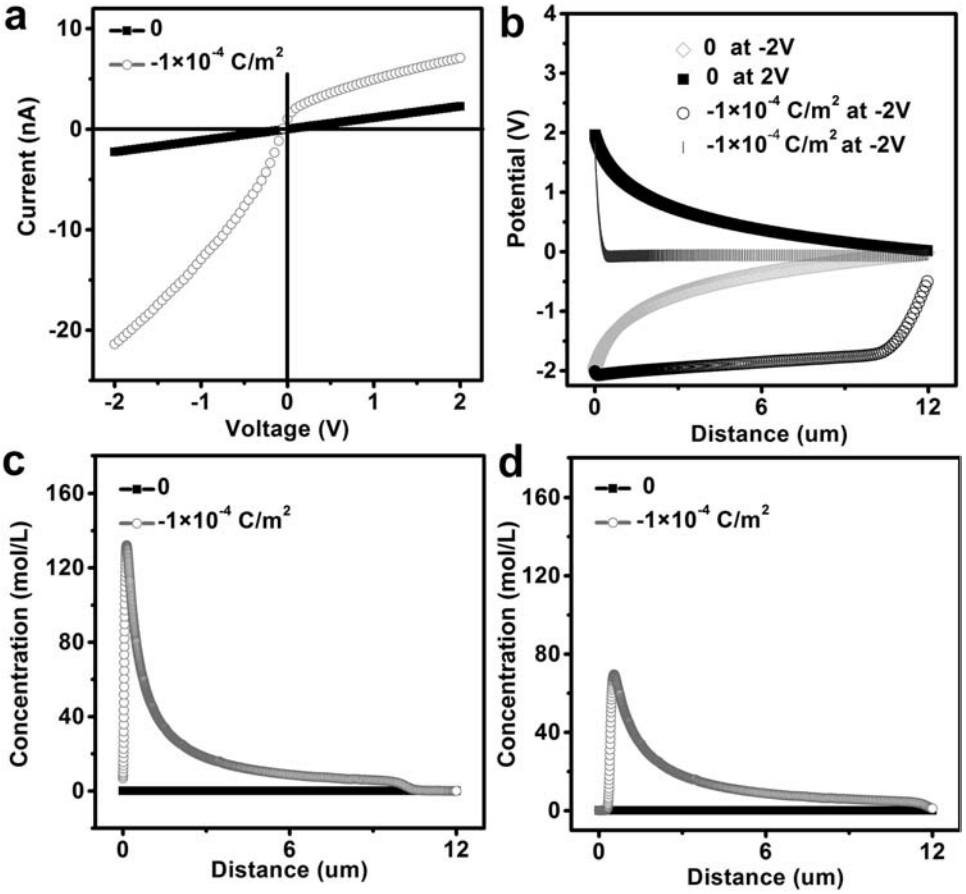

Figure 5. a) Simulated *I–V* curve of the nanochannel before and after bubbling CO. (Here, when the CO is applied to nanosystem, the surface density is defined as -1×10^{-4} C m^{-2}. Before bubbling CO, the surface charge is reduced to minimum and the surface density close to zero.) The simulated results accord with the experimental results based on the Poisson and Nernst–Planck equations. b) Potential distributions in the nanochannel when the applied external voltage is −2 and 2 V before and after bubbling CO. Before bubbling CO, the electric potential distributions are uniform. After bubbling CO, potential distribution turns to nonuniformity. The negative surface charge plays a key role in the electric potential distribution, which leads to the nonuniformity of cation and anion concentration distribution. c) Cation concentration distribution along the nanochannel at −2 V before and after bubbling CO. d) Cation concentration distribution along the nanochannel at 2 V before and after bubbling CO. Cation concentration accumulates to a higher degree at −2 V than that at 2 V near the tip of the nanochannel. Therefore, the conductance is higher under the negative bias.

Information). The small size pores (tip, 10 nm) were calculated by an electrochemical measurement result and big pore sizes.

Chemical Modification: The multiple nanochannels were chemically modified with amino ferroporphyrin on the inner surface of the nanochannels through the coupled reaction. The precursor amino porphyrin was synthesized by sequential nitration and reduction of tetraphenylporphyrin according to the literature.[20] Afterward, the amino porphyrin and $FeCl_2$ were refluxed in *N,N*-dimethylformamide (DMF) for 2 d under nitrogen atmosphere, and the amino ferroporphyrin was obtained from column separation. The total yield was very low due to the inevitable byproduct and loss during the purification. The PET nanochannels surface was activated by 1-ethyl-3-(3-dimethylaminopropyl) carbodiimide hydrochloride (100 mmol L^{-1}) in ethanol solution. The membrane was washed with deoxygenated water. Then, the membrane was added in the culture plate containing amino ferroporphyrin (10 mmol L^{-1}) for 4 h.

Current Measurement: The ion current of the CO gating anion channels were measured by a Keithley 6487 picoammeter (Keithley Instruments, Cleveland, OH). A scanning voltage was set to value from −2 to +2 V. Ag/AgCl electrodes were applied to measure ion current in the CO gating system.

Supporting Information

Supporting Information is available from the Wiley Online Library or from the author.

Acknowledgements

Y.L.X. and X.S. contributed equally to this work. This work was supported by the National Natural Science Foundation of China (21271016), the Program for New Century Excellent Talents in University, the Ph.D. Programs Foundation of the Ministry of Education of China (30400002011127001), and the Innovation Foundation of BUAA for Ph.D. Graduates.

Received: July 1, 2016
Revised: August 4, 2016
Published online: October 17, 2016

[1] a) T. Ingil, G. V. Ronnett, *J. Neurosci.* **1995**, *12*, 8214; b) M. Zhuo, S. A. Small, E. R. Kandel, R. D. Hawkins, *Science* **1993**, *260*, 1946; c) C. Thiemermann, *Nat. Med.* **2001**, *7*, 534; d) C. Peers, M. L. Dallas, J. L. Scragg, *Commun. Integr. Biol.* **2009**, *2*, 241; e) L. Wu, R. Wang, *Pharmacol. Rev.* **2005**, *57*, 585.

[2] a) C. Peers, J. P. Boyle, J. L. Scragg, M. L. Dallas, M. M. Al-Owais, N. T. Hettiarachichi, J. Elies, E. Johnson, N. Gamper, D. S. Steele, *Br. J. Pharmacol.* **2015**, *172*, 1546; b) J. Steidle, M. Diener, *Am. J. Physiol.: Gastrointest. Liver Physiol.* **2011**, *300*, G207; c) J. H. Jaggar, C. W. Leffler, S. Y. Cheranov, D. Tcheranova, E. Shuyu, X. Y. Cheng, *Circ. Res.* **2002**, *91*, 610; d) C. Peers, *Exp. Physiol.* **2011**, *96*, 836.

[3] a) D. Boehning, C. Moon, S. Sharma, K. J. Hurt, L. D. Hester, G. V. Ronnett, D. Shugar, S. H. Snyder, *Neuron* **2003**, *40*, 129; b) T. Shimizu, D. Huang, F. Yan, M. Stranava, M. Bartosova, V. Fojtikova, M. Martinkova, *Chem. Rev.* **2015**, *115*, 6491; c) H. Braunschweig, R. D. Dewhurst, F. Hupp, M. Nutz, K. Radacki, C. W. Tate, A. Vargas, Q. Ye, *Nature* **2015**, *522*, 327.

[4] a) J. H. Jaggar, A. Li, H. Parfenova, J. Liu, E. S. Umstot, A. M. Dopico, C. W. Leffler, *Circ. Res.* **2005**, *97*, 805; b) J. P. Collman, J. I. Brauman, T. R. Halbert, K. S. Suslick, *Proc. Natl. Acad. Sci. USA* **1976**, *73*, 3333.

[5] a) H. E. Boycott, M. L. Dallas, J. Elies, L. Pettinger, J. P. Boyle, J. L. Scragg, N. Gamper, C. Peers, *FASEB J.* **2013**, *27*, 3395; b) S. H. Heinemann, T. Hoshi, M. Westerhausen, A. Schiller, *Chem. Commun.* **2014**, *50*, 3644; c) M. Althaus, M. Fronius, Y. Buchäckert, I. Vadász, W. G. Clauss, W. Seeger, R. Motterlini, R. E. Morty, *Am. J. Respir. Cell Mol. Biol.* **2009**, *41*, 639; d) S. Hou, S. H. Heinemann, T. Hoshi, *Physiology* **2009**, *24*, 26.

[6] D. R. D. Premkumar, M. A. Smith, P. L. Richey, R. B. Petersen, R. Castellani, R. K. Kutty, B. Wiggert, G. Perry, R. N. Kalaria, *J. Neurochem.* **1995**, *65*, 1399.

[7] A. Kawashima, Y. Oda, A. Yachie, S. Koizumi, I. Nakanishi, *Hum. Pathol.* **2002**, *33*, 125.

[8] a) J. Wu, H. Qu, Z. Shang, S. Tao, G. Xu, J. Wu, H. Wu, S. Zhang, *New Phytol.* **2011**, *189*, 1060; b) S. Hou, R. Xu, S. H. Heinemann, T. Hoshi, *Proc. Natl. Acad. Sci. USA* **2008**, *105*, 4039.

[9] a) G. Xie, K. Xiao, Z. Zhang, X. Kong, Q. Liu, L. P. Wen, L. Jiang, *Angew. Chem.* **2015**, *127*, 1; b) Y. Jiang, N. Liu, W. Guo, F. Xia, L. Jiang, *J. Am. Chem. Soc.* **2012**, *134*, 15395.

[10] a) X. Xie, G. N. A. Crespo, G. N. Mistlberger, E. Bakker, *Nat. Chem.* **2014**, *6*, 202; b) Y. Tanaka, C. J. Hipolito, A. S. D. Maturana, K. Ito, T. Kuroda, T. Higuchi, T. Katoh, H. E. Kato, M. Hattori, K. Kumazaki, T. Tsukazaki, R. Ishitani, H. Suga, O. Nureki, *Nature* **2013**, *496*, 247.

[11] J. Gao, W. Guo, D. Feng, H. Wang, D. Zhao, L. Jiang, *J. Am. Chem. Soc.* **2014**, *136*, 12265.

[12] a) I. Hijazi, T. Roisnel, M. Fourmigué, J. Weiss, B. Boitrel, *Inorg. Chem.* **2010**, *49*, 3098; b) I. Hijazi, T. Roisnel, P. Even-Hernandez, E. Furet, J. Halet, O. Cador, B. Boitrel, *J. Am. Chem. Soc.* **2010**, *132*, 10652.

[13] a) G. P. Royer, G. M. Anantharmaiah, *J. Am. Chem. Soc.* **1979**, *12*, 3396; b) G. H. Loew, R. F. Kirchner, *Int. J. Quantum Chem.* **1978**, *5*, 403.

[14] S. W. Ryter, *Physiol. Rev.* **2006**, *86*, 583.

[15] M. M. Brooks, *Am. J. Pathol.* **1933**, *104*, 139.

[16] J. Wang, M. Zhang, J. Zhai, L. Jiang, *Phys. Chem. Chem. Phys.* **2014**, *16*, 23.

[17] a) H. Li, F. Lai, *Soft Mater.* **2013**, *11*, 13; b) Y. Ma, L. Yeh, C. Lin, L. Mei, S. Qian, *Anal. Chem.* **2015**, *87*, 4508.

[18] M. Jia, T. Kim, *Anal. Chem.* **2014**, *86*, 7360.

[19] P. Y. Apel, Y. E. Korchev, Z. Siwy, R. Spohr, M. Yoshida, *Nucl. Instrum. Methods Phys. Res., Sect. B* **2001**, *184*, 337.

[20] a) A. D. Adler, F. R. Longo, J. D. Finarelli, J. Goldmacher, J. Assour, L. Korsakoff, *J. Org. Chem.* **1966**, *32*, 476; b) W. J. Kruper, T. A. Chamberlin, M. Kochanny, *J. Org. Chem.* **1989**, *54*, 2753.